Materials Science and Engineering A 527 (2010) 4624–4632

Contents lists available at ScienceDirect

Materials Science and Engineering A

journal homepage: www.elsevier.com/locate/msea

Mechanical properties as a function of microstructure in the new Mg–Al–Ca–La alloy solidified under different conditions

Thiago V. Ferri[a], Arlan P. Figueiredo[a], Carlos R.F. Ferreira[a], Wilson Hormaza[b], Carlos A. Santos[c], Jaime A. Spim[a,*]

[a] Foundry Laboratory, Department of Metallurgy, Federal University of Rio Grande do Sul, Av. Bento Gonçalves, 9500, CEP 91501-970, Porto Alegre, RS, Brazil
[b] Faculty of Engineering, Universidad de los Andes, Bogotá D.C., Colombia
[c] Faculty of Engineering, Pontifical Catholic University of Rio Grande do Sul, Av. Ipiranga, 6681, CEP 90.619-900, Porto Alegre, RS, Brazil

ARTICLE INFO

Article history:
Received 10 November 2009
Received in revised form 4 March 2010
Accepted 11 March 2010

Keywords:
Magnesium alloy
Mechanical properties
Solidification
Macrostructure
Microstructure

ABSTRACT

This paper aimed the study of the ZAXLa05413 magnesium alloy (Mg–0.5wt%Zn–4wt%Al–1wt%Ca–3wt%La) by analyzing the influence of solidification parameters on mechanical properties. In this way the studied alloy was solidified under slow cooling condition in order to make a thermal analysis and to obtain a completely equiaxial macrostructure, in the other hand, under a unidirectional solidification condition to obtain columnar and equiaxial structures. The ingots were submitted to metallographic analysis (macro and microstructure), mechanical characterization by tensile testing and hardness measurements in specimens extracted at different positions along the height of the ingot. Expressions correlating the mechanical behavior with microstructure parameters were determined permitting the establishment of general correlations among grain size and secondary dendritic arm spacing with solidification processing variables. The results confirm a direct correlation between the structural refinement (macro and micro) and the increase in ultimate tensile strength (σ_u) and also the yield strength (σ_e) of the magnesium alloy ZAXLa05413.

1. Introduction

Electronics manufacturers, automobiles and aerospace industries are researching the advantageous properties of magnesium alloys, such as: lightweight, high corrosion resistance, electromagnetic shielding and so on. The grow rate of such alloys is predicted to be 7% annual in the next 10 years [1]. The most common magnesium alloy employed in die-casting manufacturing process is the AZ 91 (Mg–9 wt% Al–1 wt% Zn), which shows excellent mechanical properties at room temperature [2–5]. In mechanical components applications that operate in high temperature environments, such as combustion engines, is necessary the development of magnesium alloys with good creep resistance. The AE42 magnesium alloy, with the addition of rare earths (Mg–4 wt% Al–2 wt% RE), has good creep resistance compared to AZ91 alloy [3,6,7]. According to a recent paper by Anyanwu and collaborators [8], the substitution of rare earths elements by lanthanum (La), results in better creep resistance.

The metallurgical and mechanical aspects that control the microstructure are determinant as parameters in mechanical strength and ductility of cast metals. The alloy has an individual grain and a dendritic network that varies with the solute content. Second phase dispersions, porosities, boundary grain and inclusions that are formed during manufacturing process can make an obstacle to slippage while mechanical load are applied.

It is well known that as soon as the grain size becomes smaller, there is a tendency of the mechanical strength to increase at room temperature [9]. Specifically in this regard, the Hall–Petch equation can be mentioned, in which it has been established a relationship between the yield strength and the mean grain size [10–12], given by Eq. (1):

$$\sigma_e = \sigma_o + k.d^{-1/2} \quad (1)$$

where σ_e is the yield strength (MPa), σ_o is the lattice friction factor (MPa), k is the measure of the extent of stacking discordances constant and d is the average diameter of the grains (μm). This equation is not valid for polycrystalline materials that have very large or very small grain size. For cast metals, however, strength does not always increase as the grain size becomes smaller. Strength will increase with smaller grain size only if the small grains production does not increase the amount of micro porosity, the volume percentage of the second phases or the dendritic spacings.

* Corresponding author at: Foundry Laboratory, Department of Metallurgy, Federal University of Rio Grande do Sul, Av. Bento Gonçalves, 9500, CEP 91501-970, Porto Alegre, RS, Brazil. Tel.: +55 51 3308 6142.
E-mail address: spim@ufrgs.br (J.A. Spim).

0921-5093/$ – see front matter © 2010 Elsevier B.V. All rights reserved.
doi:10.1016/j.msea.2010.03.041

Table 1
Chemical composition of ZAXLa05413 magnesium alloy (wt%).

Element	Specification (%)	Measured (%)
Zinc	0.50 max	0.10
Aluminum	3.80–4.50	4.15
Calcium	0.80–1.00	1.13
Lanthanum	3.20–3.90	3.00
Magnesium	Balance	Balance

Many studies have been reported describing the relationship between structure and mechanical properties. Recent articles investigated the influence of solidification conditions on the ductility and tensile strength for the Al–Cu, Zn–Al and Al–Si alloys [13–16]. However, there are not many studies discussing this subject for magnesium alloys, and little is understood about the behavior of the solidification variables in the formation of the structures and mechanical properties.

Expressions correlating the mechanical behavior with microstructure parameters are very useful for a previous planning of the solidification conditions in terms of a determined level of mechanical resistance [13]. Therefore, correlating the yield strength (σ_e), ultimate tensile strength (σ_u) and elongation (δ) with secondary dendritic spacing (λ_2), grain size and solidification variables of the ZAXLa05413 magnesium alloy shall be very useful. In this context, the objective of the present work is to study the solidification, structural formation and mechanical properties of ZAXLa05413 magnesium alloy (Mg–0.5 wt% Zn–4 wt% Al–1 wt% Ca–3 wt% La).

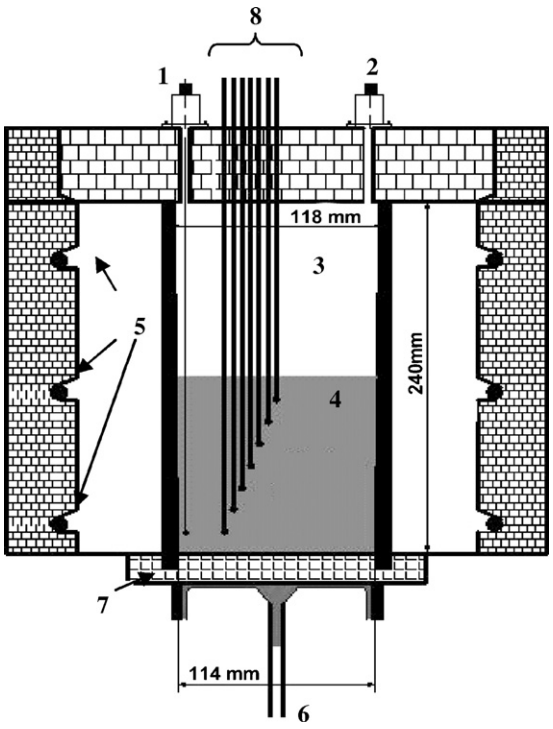

Fig. 1. Schematic representation of experimental casting arrangement: (1) auxiliary input thermocouple; (2) inlet of the mixture with argon gas and SF_6 for melting protection; (3) gas protection; (4) melt; (5) electric resistance; (6) water input; (7) cooled and uncooled bottom chill; (8) thermocouples into the melt.

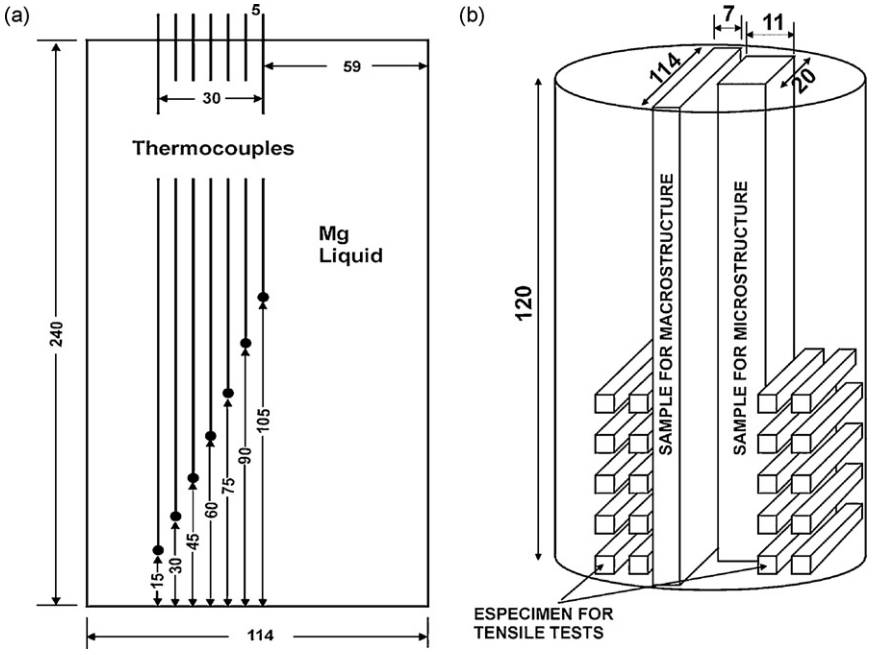

Fig. 2. (a) Position of thermocouples in the metal (mm) and (b) extracted samples for analysis: macrostructure, microstructure and tensile tests.

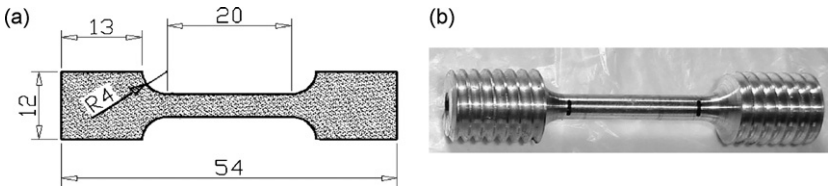

Fig. 3. (a) The specimen for tensile test according to ASTM B557 and (b) the picture of the specimen.

Table 2
Experimental conditions.

Conditions		Cooling	Pouring temperature
1	Isothermal	Air	760 °C
2	Unidirectional	Water	786 °C
3	Unidirectional	Water	789 °C

2. Experimental procedure

These experiments were performed with ZAXLa05413 magnesium alloy produced by a Brazilian company, whose chemical composition is presented in Table 1 (the average values were obtained by five measurements by ICP-OES: Inductively Coupled Plasma Spectroscopy).

A completely resistance-type electric closed furnace with a protective gas atmosphere (a mixture of SF_6 and argon gas) was designed to prevent any oxygen from coming into contact with casted magnesium to avoid the ignition of the alloy [17,18]. The alloy was melted until the molten metal reached a predetermined temperature (pouring temperature) with a superheat temperature of about 23% of the liquidus temperature for condition 1 and 28% for conditions 2 and 3. A schematic representation of the assembly used in solidification experiments is presented in Fig. 1 [19,26,27].

In order to investigate the influence of microstructure on mechanical properties, two different cooling conditions were used: isothermal and unidirectional. The isothermal condition was obtained by powering-off the furnace when the metal reached the desired temperature. To promote unidirectional heat flow during solidification, a low carbon steel (SAE/AISI 1010) water-cooled base mold was used. The use of this experimental configuration allows the minimization of natural convection, as well as solute convection due to buoyancy forces, if the rejected solute has a higher density than the melt alloy. Moreover, the casting weight will also contribute to a better metal/mold thermal contact, if lateral contraction is effective (allowing the gradual detachment of the ingot from the side walls) [20].

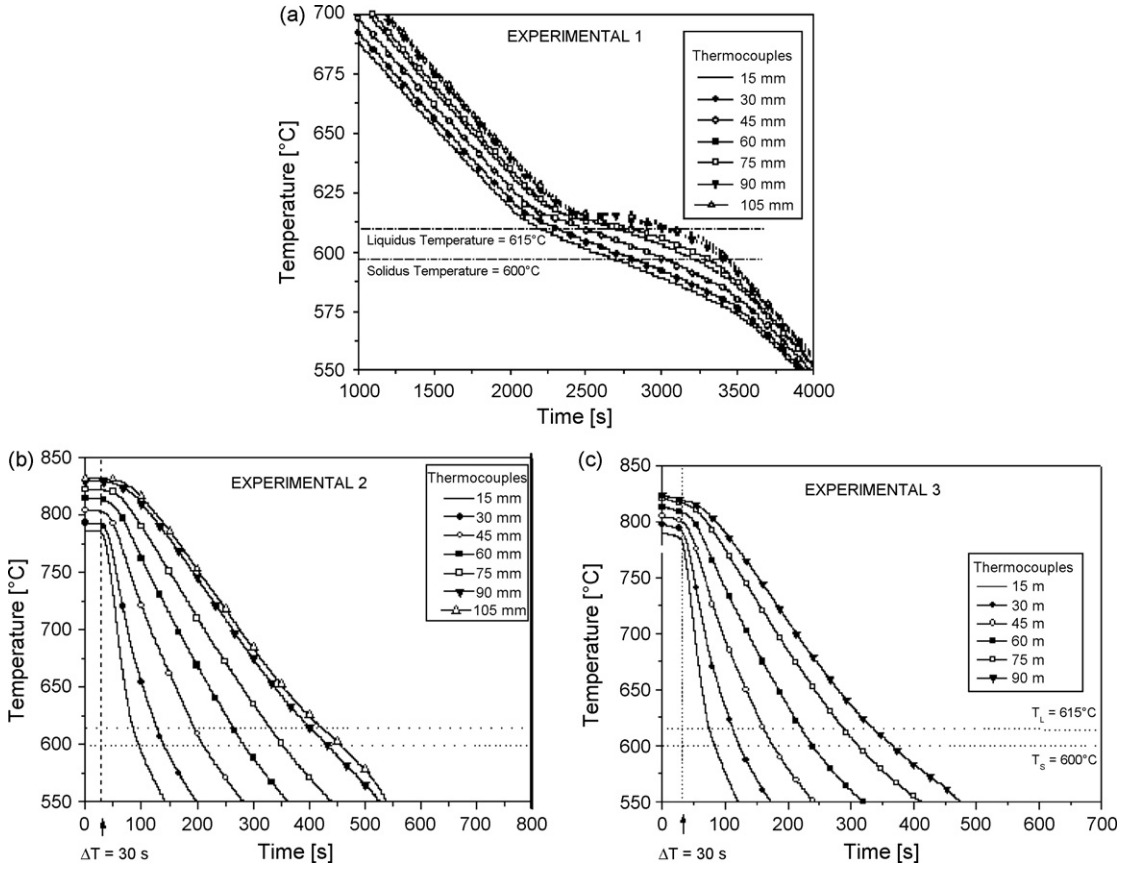

Fig. 4. Experimental thermal responses of thermocouples at different locations: (a) condition 1; (b) condition 2; (c) condition 3.

Table 3
Solidification parameters: cooling rate ($\dot{T}_L$), growth rate (V_L) and thermal gradient (G_L).

Pos (mm)	Condition 1			Condition 2			Condition 3		
	$\dot{T}_L$ (K/s)	V_L (mm/s)	G_L (K/mm)	$\dot{T}_L$ (K/s)	V_L (mm/s)	G_L (K/mm)	$\dot{T}_L$ (K/s)	V_L (mm/s)	G_L (K/mm)
10	0.074	0.47	0.16	3.54	0.26	13.7	4.07	0.32	12.6
30	0.075	0.32	0.24	1.85	0.24	7.8	2.26	0.29	7.8
45	0.077	0.26	0.30	1.21	0.22	5.5	1.48	0.26	5.6
60	0.078	0.20	0.40	0.90	0.21	4.3	1.09	0.25	4.4
75	0.076	0.16	0.47	0.75	0.20	3.7	0.84	0.23	3.6
90	0.076	0.13	0.57	0.65	0.20	3.3	–	90	0.74
105	0.074	0.13	0.57	0.63	0.20	3.2	–	105	–

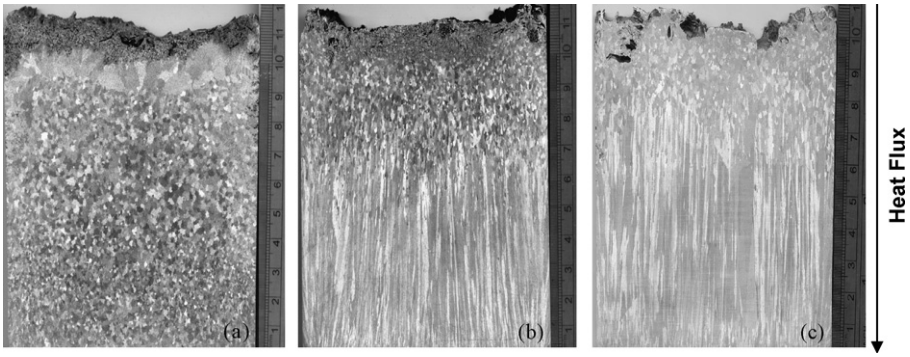

Fig. 5. Macrostructure ZAXLa05413 ingots: (a) condition 1; (b) condition 2; (c) condition 3.

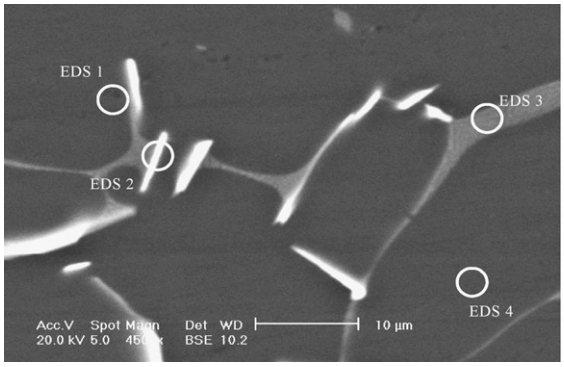

Region	Mg	Al	Ca	La
EDS 1 – close to grain boundary	94.4	4.0	0.5	0.9
EDS 2 – acicular phase	71.8	12.4	0.0	15.7
EDS 3 – lamellar phase	71.9	16.0	11.9	0.0
EDS 4 – inner grain	100.0	0.0	0.0	0.0

Fig. 6. Scanning electron microscopy image of cast specimen ZAXLa05413 and results of the elemental composition obtained by Energy Dispersive X-Ray Spectroscopy (wt%).

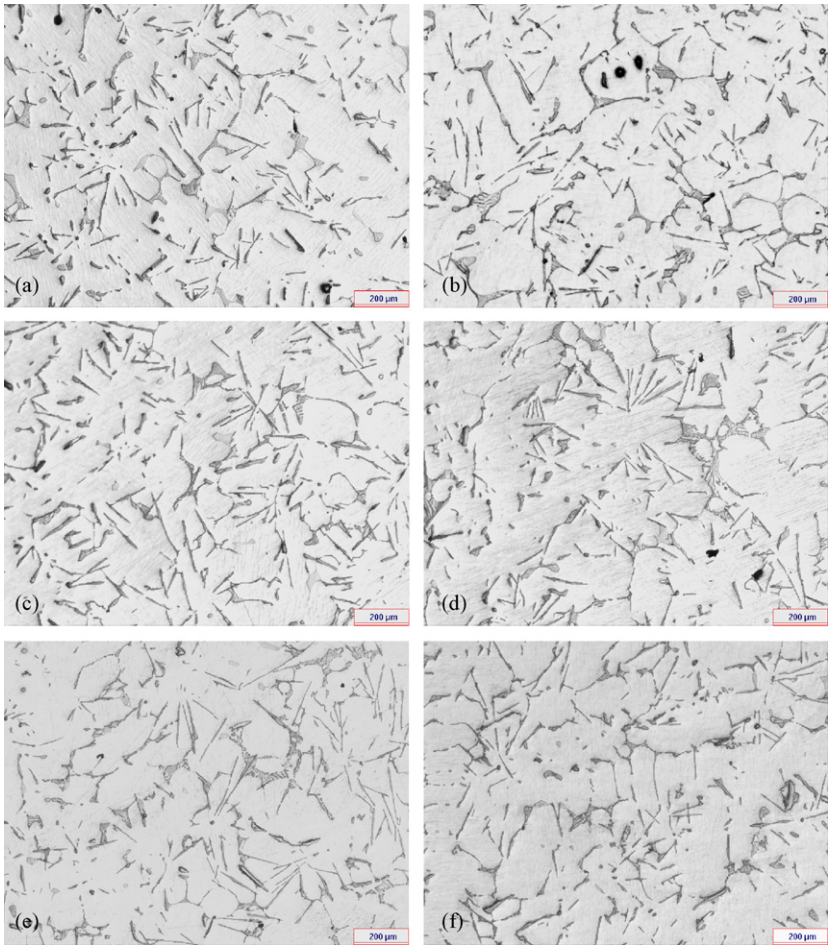

Fig. 7. Microstructure of the alloy in condition 1: (a) 15 mm; (b) 30 mm; (c) 45 mm; (d) 60 mm; (e) 75 mm; (f) 90 mm from the metal/mold interface.

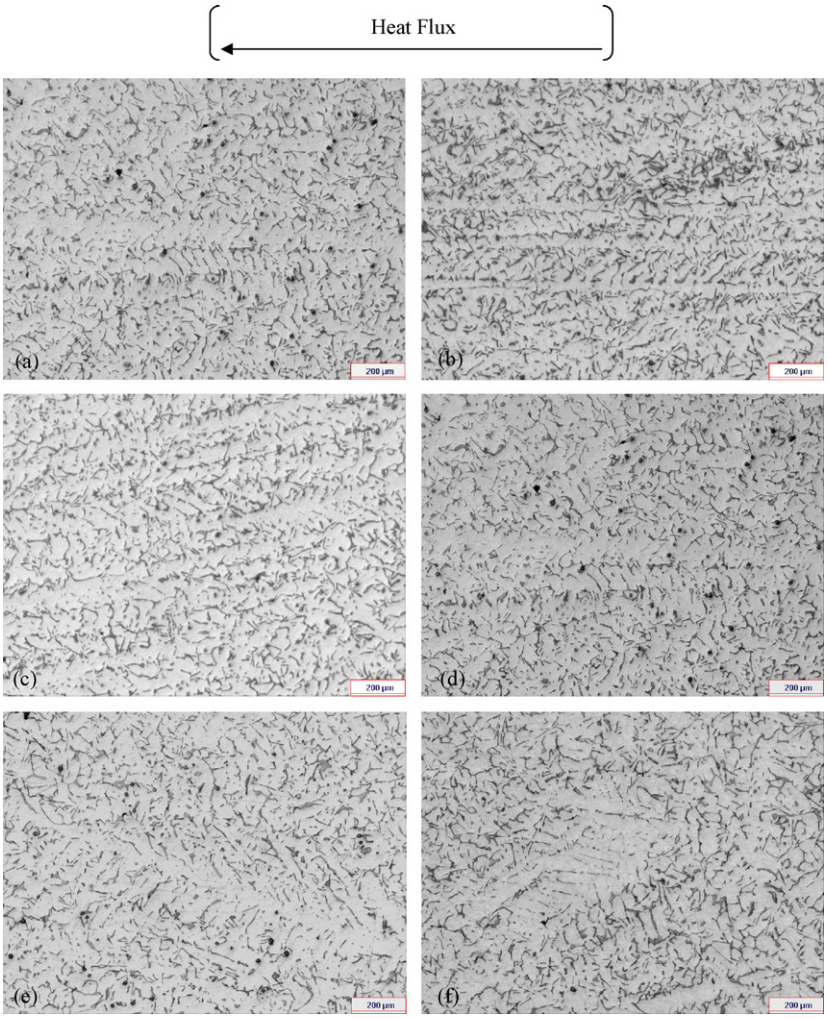

Fig. 8. Microstructure of the alloy in condition 2: (a) 15 mm; (b) 30 mm; (c) 45 mm; (d) 60 mm; (e) 75 mm; (f) 90 mm from the metal/mold interface.

Table 4
Mechanical properties for the condition 1.

Distance from the metal/mold interface	σ_u (MPa)	$\sigma_{0.2}$ (MPa)	ε (%)	Grain size (μm)	Hardness (HB)
15 mm	57.5 ± 2.6	54.0 ± 2.6	1.2 ± 0.17	1310 ± 406	67.5 ± 2.5
30 mm	58.6 ± 1.5	54.0 ± 1.4	1.3 ± 0.14	1490 ± 465	66.6 ± 2.3
45 mm	56.2 ± 2.6	48.7 ± 6.8	1.4 ± 0.05	1755 ± 489	66.6 ± 1.3
60 mm	51.3 ± 3.6	46.2 ± 3.6	1.4 ± 0.19	2143 ± 576	65.5 ± 1.9
75 mm	51.0 ± 11.5	48.2 ± 10.7	1.3 ± 0.13	2560 ± 685	64.7 ± 1.7

Temperatures in the casting were monitored during solidification by a bank of type K thermocouples (1.6 mm diameter, AISI/SAE 446 chromium-steel) accurately positioned respecting the metal/mold interface, as indicated in Fig. 2a. The temperature data was used to estimate solidification parameters such as growth rate, thermal gradient and cooling rate. Growth rate (V_L) was obtained by the time of liquidus isotherm between two adjacent thermocouples [13,14,21].

In order to analyze the macrostructure, a longitudinal sample was sectioned from the center of the ingot (7 mm thick, 114 mm wide and 120 mm high – Fig. 2b), then polished and etched to reveal the macrostructures. The reagent used was a solution containing 20% acetic acid in water. Additionally an image analysis system (OMNIMET© ENTERPRISE) was applied to measure grain size.

In the microstructure analysis, a longitudinal sample was extracted close to thermocouple positions (11 mm thick, 20 mm

Table 5
Mechanical properties for the condition 2.

Distance from the metal/mold interface	σ_u (MPa)	$\sigma_{0.2}$ (MPa)	ε (%)	λ_2 (μm)	Hardness (HB)
15 mm	102.0 ± 4.2	92.7 ± 3.8	1.7 ± 0.17	41.8 ± 4.0	80.4 ± 5.5
30 mm	93.7 ± 1.7	89.0 ± 4.0	1.5 ± 0.16	50.6 ± 5.3	74.0 ± 1.5
45 mm	93.2 ± 7.0	81.5 ± 4.5	1.5 ± 0.11	61.0 ± 5.7	73.5 ± 2.6
60 mm	93.7 ± 5.0	76.5 ± 6.8	1.7 ± 0.17	69.0 ± 4.7	72.6 ± 2.0
75 mm	88.2 ± 5.0	74.4 ± 4.0	1.5 ± 0.05	70.7 ± 7.7	70.8 ± 3.2

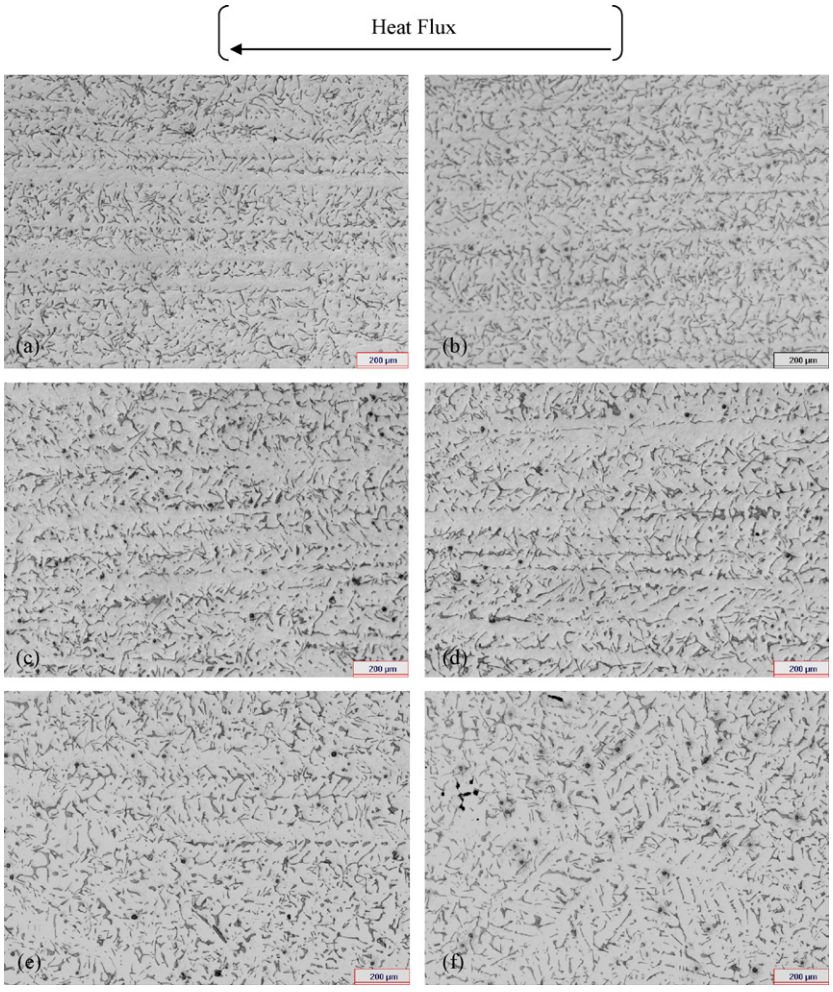

Fig. 9. Microstructure of the alloy in condition 3: (a) 15 mm; (b) 30 mm; (c) 45 mm; (d) 60 mm; (e) 75 mm; (f) 90 mm from the metal/mold interface.

wide and 120 mm high – Fig. 2b). Three specimens were extracted from the sample along the height. The specimens were ground and analyzed without etching.

Transversal samples were sectioned from casting, as indicated in Fig. 2b, and prepared for tensile testing according to ASTM Standard B557-02[a] specifications, as shown in Fig. 3 [22]. A specific claw was design, in order to perform the tests, which were performed using an EMIC DL-500B device machine, with 2000 kgf maximum force, 0.02–500 mm/min velocity and 500 kgf load cell. To ensure reproducibility of results, four specimens were tested for each selected position (20 specimens per ingot), and mean values of yield strength, ultimate tensile strength, elongation and hardness were determined at different positions respecting the metal/mold interface. The positions were: 15, 30, 45, 60 and 75 mm from the bottom (the same as the thermocouples). Brinell hardness tests were performed in the transversal specimens according to ASTM E 10-07 [23].

3. Results and discussion

The initial conditions of solidification are shown in Table 2. In condition 1, the slow solidification was performed to get as close as possible to the thermodynamic equilibrium condition allowing the determination of the liquidus (T_L) and solidus (T_S) temperatures. On the other hand, under conditions 2 and 3, upward unidirectional solidification was performed to obtain preferential dendritic growth in the opposite direction of the heat extraction, and also to evaluate the influence of structural behavior on mechanical properties.

Fig. 4 shows the cooling curves obtained by the thermocouples under conditions 1, 2 and 3, respectively. The thermal analysis of condition 1 (isothermal) allowed the determination of the liquidus temperature (T_L) at approximately 615 °C and the solidus temperature (T_S) at 600 °C, characterizing a narrow range of mushy zone

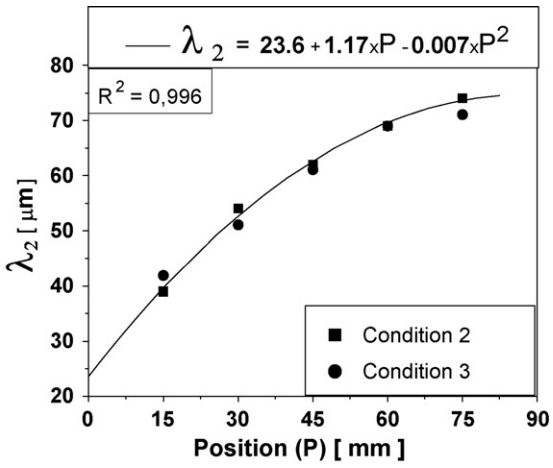

Fig. 10. Variation of the secondary dendritic spacing (λ_2) as a function of the distance from the metal/mold interface for conditions 2 and 3.

of 15 °C. The values of the cooling rates, growth rates and thermal gradients for conditions 1, 2 and 3 are shown in Table 3.

Macrographs obtained from the experiments are shown in Fig. 5. For the first condition, the equiaxed macrostructure was formed along the entire length of the ingot and as closest the structure gets to the top coarser the structure gets. In the other two conditions the macrostructures formed are similar, showing refined columnar grains growing in the opposite direction to the heat extraction from the bottom towards to the top of the ingot. In both ingots the columnar to equiaxed transition (CET) was observed near to slag formation (~700 mm and 800 mm, respectively).

The effect of lanthanum and aluminum addition, provoked the crystallization of a large amount of acicular compounds ($Al_{11}La_3$) across the grain boundaries which are more stable and constitute an effective obstacle to grain slippage [8]. The addition of Ca content of from 0 to 2 wt% in Mg and 5 wt% in Al was researched in respect to the formation of the lamellar phase (Al_2Ca) [24]. The addition of the Ca tends to reduce secondary dendritic arm spacing (λ_2) and β-phase formation ($Mg_{17}Al_{12}$). When the Ca contents is above 1.5 wt% the β-phase is replaced by the $(Al,Mg)_2Ca$ phases and Al_2Ca phase locates preferentially in the boundaries of the grain.

The alloy studied in this work also presented needles of lanthanum (acicular phase $Al_{11}La_3$) in all directions and around the grain contours. Also the lamellar phase Al_2Ca is presented along grain boundaries. Scanning electron microscopy (SEM) micrographs of cast specimen can be observed in Fig. 6. The elemental composition of the phases were determined using Energy Dispersive X-ray Spectroscopy (EDS), which showed the following: EDS 1 and EDS 4 – Mg matrix with Al, Ca and La into solid solution, EDS 2 – acicular phase with La and Al, and EDS 3 – lamellar phase with Ca and Al.

The micrographs obtained by optical microscopy are shown in Figs. 7–9. The microstructures presented in Figs. 7–9 show that the white phase is the magnesium matrix and also the acicular phases in all directions represent the lanthanum needles (EDS 2 – $Al_{11}La_3$). Another microstructure composed of lamellar precipitations was found predominantly near the grain boundaries, which possibly represent the formation of Al_2Ca, according to EDS 3.

In condition 1 it was impossible to visualize directional dendritic growth because the slow and gradual solidification do not influence the dendritic growth direction, making it difficult to visualize the secondary dendritic arm spacing (λ_2). On the other hand, for conditions 2 and 3 it was possible to conclude that the secondary dendritic arm spacing (λ_2) had similar results as well as the macrostructural formation.

The microstructures of the condition 1, shown in Fig. 7 had a coarser grained than the microstructures of the conditions 2 and 3, which makes easier to observe the phases formed. Because the microstructures formed in conditions 2 and 3 were more refined, it was difficult to observe the formed phases, especially the lamellar phases. However, dendritic refinement and preferential direction of growth allowed the measurement of the secondary dendritic arm spacing. The dendritic arm spacing presented higher refinement near to the heat extraction base and the spacing increase as it moves away from this base, as shown in Figs. 8 and 9 respectively.

In the microstructure of Fig. 9(f), the formation of rosette-shaped dendrite can be seen, which shows the lack of directional dendritic growth caused by low heat extraction represented in the CET region.

The mechanical properties obtained for the conditions 2 and 3 resulted in similar values of magnitude along the ingot, which was already expected due to the similarity between macrostructures and microstructures. The microstructure of secondary dendritic arm spacing (λ_2) along the ingot for the conditions 2 and 3 can be considered similar, as shown in Fig. 10.

The Tables 4 and 5 present the results of conditions 1 and 2 with the following parameters: ultimate tensile strength (σ_u), yield strength (σ_e), specific elongation (δ), obtained from 4 specimens extracted from the same region (height of the ingot), mean grain

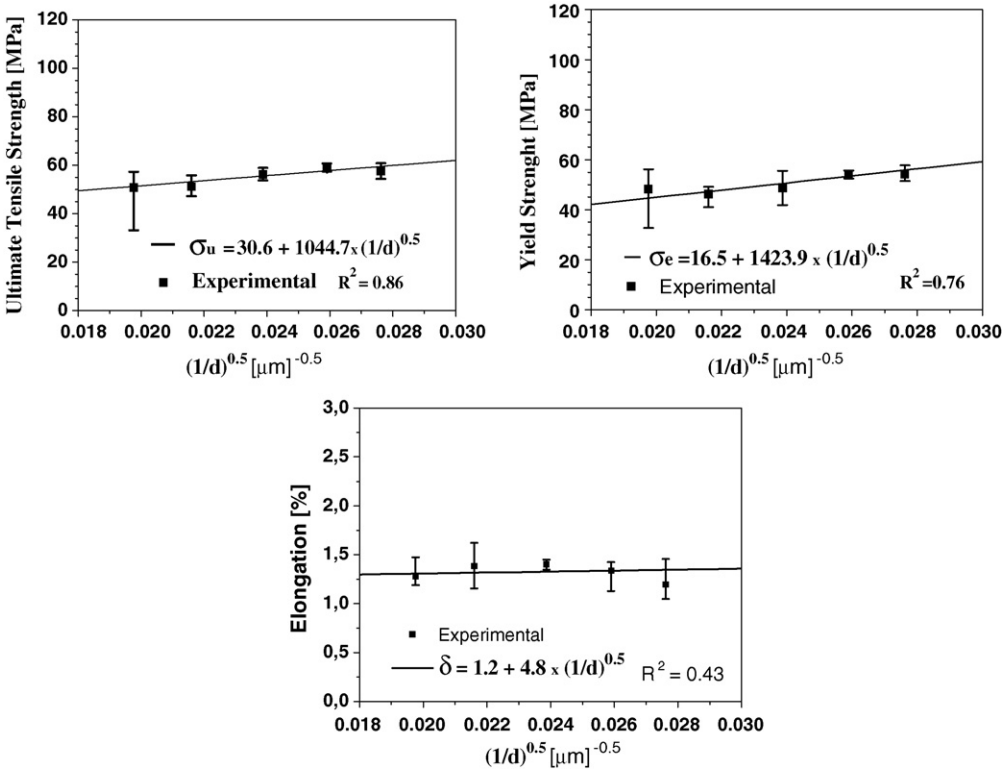

Fig. 11. Correlation between mechanical properties and average grain size for the condition 1.

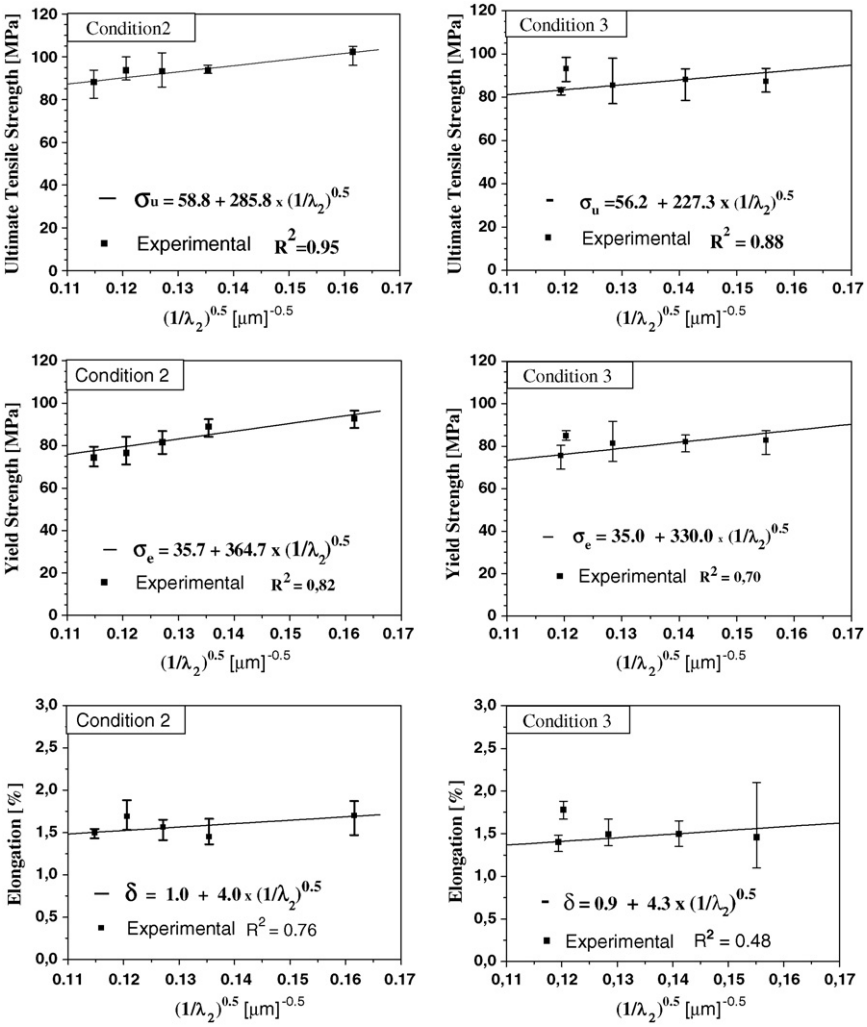

Fig. 12. Correlation between mechanical properties and secondary dendritic arm spacing for the conditions 2 and 3.

size and hardness for the condition 1 and the dendritic spacings for condition 2.

The mean, the maximum and the minimum values of the mechanical properties obtained during the tensile tests are plotted in Figs. 11 and 12. The experimental results obtained using previous tests showed the relationship established between mechanical properties (σ_u, σ_e, δ) and the inverse square root on the mean diameter of the grains it is only true in the condition 1 (Fig. 11).

In the conditions 2 and 3 the relationship is between mechanical properties (σ_u, σ_e, δ) and the inverse secondary dendritic spacing (λ_2) as can be seen in Fig. 12.

The empirical equations correspond to the best fit between mechanical properties along the ingot and the structural parameters are plotted into the graphs shown in Figs. 11 and 12.

Comparison of the conditions 1, 2 and 3 showed an increase of ultimate tensile strength (σ_u) and tensile yield strength (σ_e) as the cooling rate increased [25]. The lowest levels of strength properties were observed in condition 1 (low cooling rate). The strength properties of the conditions 2 and 3 were higher and similar.

An increase in mechanical strength in the magnesium alloy ZAXLa05413 with macrostructural refinement (grain size) follows the Hall–Petch law. There is also an effective correlation between microstructural refinement (secondary dendritic arm spacing) and the enhancement of the mechanical properties.

It is observed that the correlation of tensile yield strength with the metallurgical characteristics, average grain size and spacing of dendrites, has become more realistic due to lower levels of strain. For the relationships of ultimate tensile strength and specific elongation, other factors related to significant plastic deformation due to higher levels of plastic strain involved may influence the results as well.

4. Conclusions

ZAXLa05413 magnesium alloy showed a direct relationship between macrostructural (grain size) and microstructural refinement (secondary dendritic arm spacing), with an increase in mechanical properties represented by empirical equations.

The data obtained showed that ZAXLa05413 magnesium alloy has appropriate manufacturing conditions where there is high heat extraction, as in the case of the die-castings. The high heat extraction rates could be linked to a greater tendency for macro and microstructural refinement of ZAXLa05413 resulting in higher mechanical properties.

Acknowledgements

The authors acknowledge financial support provided by CNPq (The Brazilian Research Council), FAPERGS (The Scientific Research Foundation of the State of Rio Grande do Sul) and the Brazilian Company – STIHL.

References

[1] B.L. Mordike, T. Ebert, Mater. Sci. Eng. A 302 (1) (2001) 37–45.
[2] E.M. Gutman, Y. Unigobski, M. Levkovitch, Z. Koren, Mater. Sci. Eng. A 234–236 (1997) 880–883.
[3] J. D. Sakkinen, Physical metallurgy of magnesium die cast alloys, Society of Automotive Engineers – SAE. Technical Papers 940779, 1994, pp. 71–82.
[4] M. Vogel, O. Kraft, E. Arzt, Scripta Mater. 48 (8) (2003) 985–990.
[5] Z. Zhang, R. Tremblay, D. Dube, Mater. Sci. Eng. A 385 (1–2) (2004) 286–291.
[6] I.P. Moreno, T.K. Nandy, J.W. Jones, J.E. Allison, T.M. Pollock, Scripta Mater. 45 (12) (2001) 1423–1429.
[7] B.R. Powell, V. Rezhets, M.P. Balogh, R.A. Waldo, J. Min. Met. Mater. Soc. JOM 54 (2002) 34–38.
[8] I.A. Anyanwu, S. Kamado, T. Honda, Y. Kojima, S. Takeda, T. Ishida, Mater. Sci. Eng. A 380 (2004) 93–99.
[9] C.D. Lee, Mater. Sci. Eng. A 459 (1–2) (2007) 355–360.
[10] E.O. Hall, Proc. Phys. Soc. 71B (1951) 454–747.
[11] N.J. Petch, J. Iron Steel Inst. 174 (1953) 25–35.
[12] A.N. El-Mahallawy, M.A. Taha, E. Pokora, F. Klein, J. Mater. Process. Technol. 73 (1–3) (1998) 125–138.
[13] J.M.V. Quaresma, C.A. Santos, A. Garcia, Metall. Mater. Trans. A (2000) 3167–3178.
[14] W.R.R. Osório, A. Garcia, Mater. Sci. Eng. A 325 (1–2) (2002) 103–111.
[15] W.R.R. Osório, C.A. Santos, J.M.V. Quaresma, A. Garcia, J. Mater. Process. Technol. 143 (2003) 703–709.
[16] P.R. Goulart, J.E. Spinelli, W.R.R. Osorio, A. Garcia, Mater. Sci. Eng. A 421 (1–2) (2006) 245–253.
[17] N.V.B. Ravi Kumar, M. Suery, E. Grosjean, Scripta Mater. 49 (3) (2003) 225–230.
[18] T.S.W. Shih, Jing-Hwe, K.Z. Chong, Mater. Chem. Phys. 85 (2–3) (2004) 302–309.
[19] T.V. Ferri, Caracterização Mecânica da Liga de Magnésio ZAXLa05413 para Aplicação em Die Casting, Master Dissertation, UFRGS-Brazil, 2008.
[20] O.L. Rocha, C.A. Siqueira, A. Garcia, Mater. Sci. Eng. A 347 (1–2) (2003) 59–69.
[21] A.P. Figueiredo, Análise da Solidificação de Ligas de Magnésio para Aplicação na Fabricação de Motores, Master Dissertation, UFRGS-Brazil, 2008.
[22] ASTM-B557, Standard Test Methods of Tension Testing Wrought and Cast Aluminum and Magnesium-Alloy Products, ASTM, 2003.
[23] ASTM E 10, Standard Test Method for Brinell Hardness of Metallic Materials, ASTM, 2007.
[24] L. Han, H. Hu, D.O. Northwood, Mater. Lett. 62 (3) (2008) 381–384.
[25] L.L. Rokhlin, Magnesium Alloys Containing Rare Earth Metals: Structure and Properties, Taylor & Francis, London, 2003.
[26] T.V. Ferri, A.P. Figueiredo, C.A. dos Santos, C.R.F. Ferreira, J.A. Spim, Anais do 63°. Congresso anual da ABM, vol. 1, 2008, pp. 1277–1286.
[27] T.V. Ferri, A.P. Figueiredo, C.A. dos Santos, C.R.F. Ferreira, J.A. Spim, Anais do 63°. Congresso anual da ABM, vol. 1, 2008, pp. 1287–1298.